Role of Structure and Oxidation States in the Passivation of Stainless Steel by Chromium

Suman Bhasker Ranganath[1,2], Collin D. Wick[1], and B. Ramu Ramachandran[1*]

[1]College of Engineering & Science,
Louisiana Tech University
Ruston, Louisiana 71272, USA
*ramu@latech.edu

[2]Department of Chemical Engineering
Louisiana State University
Baton Rouge, Louisiana 70803, USA

Abstract— **The early stages of the oxidation of stainless steel is studied using first principles density functional theory calculations. A Monte Carlo approach was used to efficiently identify the most probable low energy structures in the high-dimensional configuration space. The composition, structure, and oxidation states of the atoms in the oxide layers were analyzed by atomic density profiles, nearest neighbor distribution, and Bader charge analysis. The results suggest that the passivation of steel by chromium is largely due to its high preference for the Cr^{3+} oxidation state with 6 oxygen neighbors. In contrast, iron is more susceptible to oxygen penetration because of its variable oxidation state between Fe^{2+} and Fe^{3+}, and a range nearest oxygen neighbor numbers.**

Keywords- density functional theory, stainless steel, oxidation of steel, metal passivation

I.   INTRODUCTION

Iron-chromium alloy systems have been used as models for stainless steel in various computational studies [1]–[7]. Given the difficulty of studying long-term phenomena like rusting using first principles computational methods, various approximations and simplifications have been employed to gain useful insights, and first principles approaches have necessarily been limited to the early stage phenomena.

Given the industrial and economical significance of understanding and controlling the corrosion of steel, this area has been a topic of experimental research for many decades [9]–[14], and continues to be active to this day [15]–[21]. It has been known from the earliest experiments that chromium plays a central role in the passivation of the oxidative process. However, a clear understanding of the molecular mechanisms responsible for the passivation of the oxidative process is still lacking. Recent experiments have used sophisticated surface characterization and depth profiling techniques to provide detailed information about the chemical composition and structure of the surface layers formed during the early stages of steel oxidation under low and high temperature conditions. These results suggest that lower temperature processes result in greater concentration of iron oxides at the interface with air while the oxides of chromium are dominant in the surface layers at higher temperatures.

In this paper, we present a first principles computational study of the oxide layers formed during the early stages of steel oxidation at low temperature, when the oxide layer thickness is on the order of ~1- 2 nm. An innovation introduced in our work is a Monte Carlo procedure that allows us to rapidly explore the complex energy landscape of the system and identify structures that are most likely to correspond to the lowest energy atomic configurations. The computations are initiated from four different initial configurations. It is found that the final stable configurations identified are largely independent of the starting structures, thus establishing that the Monte Carlo procedure is robust, and that the identified stable configurations are likely to be among the most stable thermodynamically. The oxide layers are then characterized chemically using nearest neighbor analysis and Bader charge analysis. These provide interesting insights into the mechanism of chromium passivation.
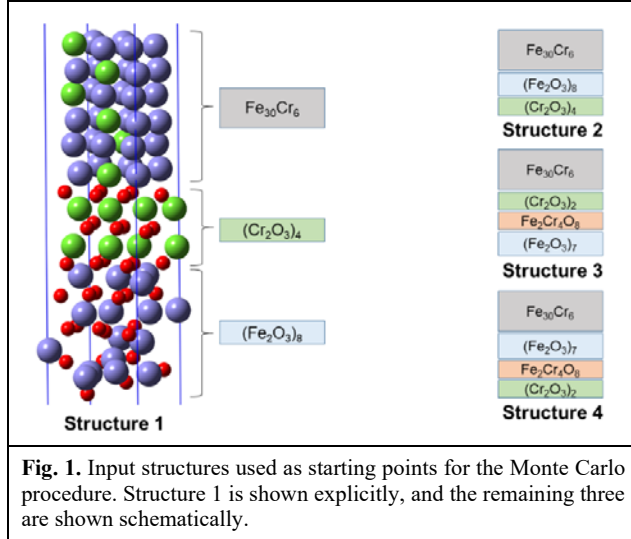
II.   COMPUTATIONAL METHODS

Total energy calculations were carried out in the framework of Kohn-Sham (KS) plane-wave density functional theory (DFT) using the Vienna Ab intio Simulation Package [22]. The Perdew, Burke and Ernzerhof (PBE) form of generalized gradient approximation [23] is used to describe the exchange-correlation energy. Potential due to core electrons is accounted by the projector augmented wave method which combines the features of pseudopotential approach and the linear augmented plane wave method [24], [25]. The KS orbitals for valence electrons are expanded in terms of plane wave basis set with 400 eV cutoff energy [26]. A k-point mesh of 2×2×1 in the Monkhorst-Pack scheme is used for sampling the first Brillouin zone [27].

The four initial structures were selected based on information provided by experimental work [10]. Six layers of Fe (001) (36 atoms) stacked in the *z*-direction (~9 Å) were matched with six layers of Fe_2O_3 (001) (60 total atoms; ~15 Å) forming an interface with Fe (001) perpendicular to the *z*-direction, and an additional 12 Å of vacuum in the *z*-direction. The pure Fe phase was in contact with the oxygen terminated oxide layer surface, which resulted in a lower energy configuration. To create the FeCr alloy, one Fe atom per layer was randomly selected and replaced with a Cr atom (or one in six atoms). Four different arrangements of Fe and Cr were used in the oxide layer to create the starting structures with layered oxides, again by replacing Fe atoms with Cr. The starting

GSTF © 2019

structures differ in the compositions of the vacuum/oxide interface, the oxide/alloy interface, and the subsurface layers. The first input structure is explicitly shown in Figure 1, along with schematics of the other three. Note that the vacuum/solid interface is at the "bottom" in this figure.

Fig. 1. Input structures used as starting points for the Monte Carlo procedure. Structure 1 is shown explicitly, and the remaining three are shown schematically.
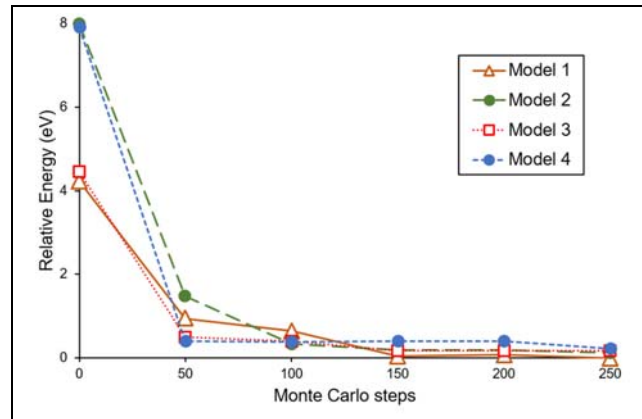
As noted in the Introduction, a Monte Carlo procedure was introduced to efficiently search the complex configuration space for lowest energy structures. The method used a Markov chain in which each successive step allowed two random Fe atoms to be exchanged with two random Cr atoms, excluding those in the two layers next to the FeCr/vacuum interface. In each step, two Fe atoms and two Cr atoms were swapped at random, followed by a geometry optimization. Four such trials were carried out from each starting structure and the structure with the lowest energy after optimization (within a window of 0.1 eV, to prevent getting trapped in local minima) was retained for further swaps. The optimization step modifies the oxide structure. Therefore, the structures evolve throughout the MC procedure. With this approach, the total energy after each step was nearly always lower than that of the structure from which it evolved. A total of 250 MC steps were employed for each.

The elemental compositions of the oxide layers were analyzed by computing atomic density profiles as a function of the vertical coordinate. The vacuum/solid interface was placed at $z = 0$ and the oxide and alloy layers at higher values of z, so that the "depth" profile could be discussed, as in the case of experimental analyses. The density profiles were computed by convoluting the atomic distribution with a Gaussian function with a width of 1 Å (see below).

The number of nearest neighbors of each atom in the oxide layers was calculated to examine how the atoms were distributed. Two atoms were considered nearest neighbors if their interatomic distance was within the first peak of their radial distribution function. Further insights into the chemical compositions of the oxide layer was obtained using Bader charge analysis [28] using the code provided by the Henkelman group [29]–[33].

III. RESULTS AND DISCUSSION

Figure 2 shows the changes in total energy as a function of the Monte Carlo swaps described above. The total energy decreased rapidly early in the swapping procedure and at a much slower rate for the remaining steps until the changes became negligible, suggesting that the identified structures were among the lowest energy configurations that could be found. The atomic density profiles of the final structures obtained from the four starting structures were found to be remarkably similar. As noted above, the relative insensitivity of the final structures to the starting structure is an indication that the Monte Carlo procedure is robust, and that the structures were allowed to evolve for sufficient numbers of steps. The structure resulting from initial structure 3 is shown in Figure 3 along with the starting structure from which it evolved. To further remove the initial structure dependence, we averaged the density profiles of all four structures, which is shown in Figure 4.

Fig. 2. The variation of total energy for each starting structure, relative to the total energy of the lowest energy structure (Model 1 at 250 steps) as a function of Monte Carlo steps.
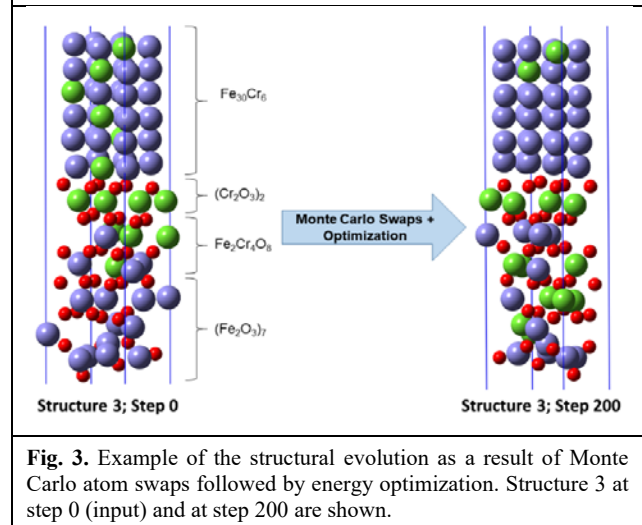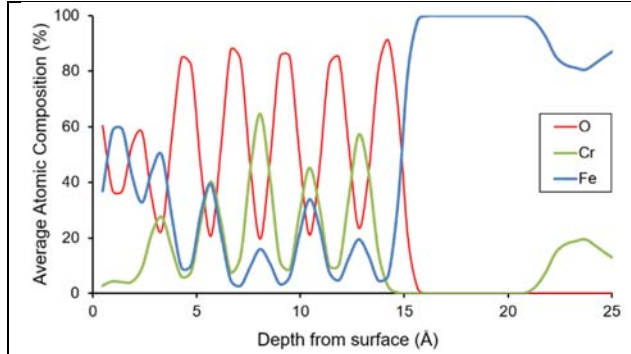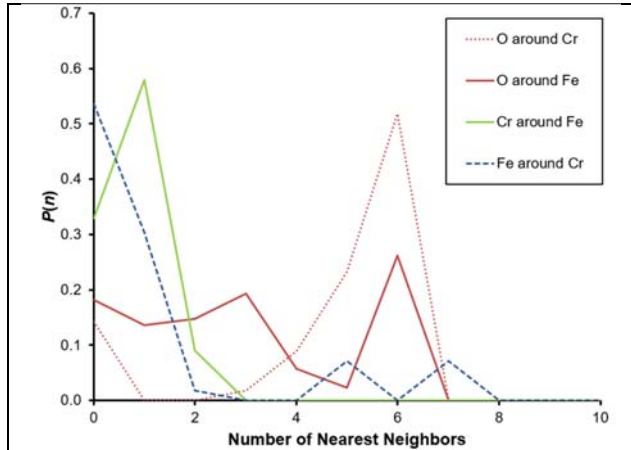

Fig. 3. Example of the structural evolution as a result of Monte Carlo atom swaps followed by energy optimization. Structure 3 at step 0 (input) and at step 200 are shown.

Figure 4 shows that the surface layer of the oxidized steel is dominated by oxides of iron, which is qualitatively consistent

11

with the findings from experiments conducted at lower temperatures. The results also strongly suggest that it was energetically favorable for Cr from the alloy phase in the 15-20 Å range to migrate into the oxide layer. The apparent depletion of Cr in the alloy layers near the alloy/oxide interface was a consequence of the alloy initial configuration and including those layers in the atom swaps. Excluding the two layers closest to the alloy/vacuum interface from swapping leaves two Cr atoms in those layers, as seen in Fig. 3 and reflected in the density profile in Fig. 4.

Fig. 4. Distribution of Fe, Cr, and O atoms averaged over the four final structures identified.

In the same spirit as Fig. 4, nearest neighbor analysis was also performed for all four final structures and averaged. The results are shown in Figure 5. The distribution $P(n)$ represents the probability of an atom to have a certain number of atoms n within a certain cut-off radius, which is based on the first peak of its radial distribution function. The cut-off radii used were as follows: O-Cr: 2.1 Å, O-Fe: 2.5 Å, and Fe-Cr: 2.5 Å.
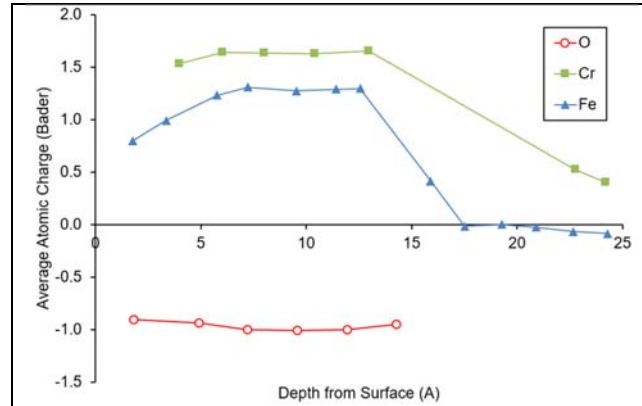

Fig. 5. Distribution of nearest neighbors of specified types, averaged over the four final structures identified.

Figure 5 shows that 75% of all Cr atoms are surrounded by 5 (23%) to 6 (52%) oxygens. In contrast, 26% of Fe has 6 oxygen neighbors, 19% has 3 oxygen neighbors, and 15% and 14% have 2 and 1 oxygen neighbors, respectively. Bulk Fe_2O_3 and Cr_2O_3 structures have 6 oxygen neighbors within the cut-off radius while bulk FeO has 3 oxygen neighbors within the cut-off radius (and one more just outside that radius). These results imply that Cr prefers to be in the Cr^{3+} oxidation state whereas Fe has almost equal preference for +3 or +2 oxidation states and also shows some structural flexibility. These conclusions are further supported by Bader charge analysis.

Bader charge analysis [28] is based on the intuitive division of total charge density in a molecule among the constituent atoms, using a dividing surface defined by connecting the points around an atom at which the charge density reaches a minimum. The charge enclosed within this volume enclosed by the dividing surface is the Bader charge, which is proportional to the oxidation state of the atom. The results of averaging the Bader charge analysis on the four final structures are presented in Figure 6, as a function of the vertical coordinate. With three exceptions (two involving Fe atoms and one involving O at the vacuum/oxide interface) the standard deviations at each value of z are smaller than or the same height as the symbol used. The error bars for the three exceptions are 2 to 4 times the height of the symbol.

Fig. 6. Bader atomic charges on O, Cr, and Fe as a function of depth from the vacuum/oxide surface. The charges have been averaged over the same atom types at a particular depth and also over the four final structures.

The Fe atoms in the bulk alloy ($z > 15$ Å) have slightly negative charges (0.0 to –0.08e) but the charges rise to 1.3-1.4e in the range $7 \leq z \leq 11$ Å and drops to lower values as the vacuum/oxide interface is approached at small values of z. In contrast, Cr charges are consistently higher than those of Fe, remaining around 1.5e, largely independent of z with in the oxide phase ($z < 15$ Å), dropping approaching 0.4-0.5e in the fixed layer of the pure alloy phase at the largest values of z. These observations are consistent with the conjecture advanced above that Fe shows more flexibility or lability in its oxidation state while Cr prefers to be in a fixed oxidation state. The oxygen atoms appear to be quite consistent in assuming –1e charge independent of z.

Considering the results of the nearest neighbor analysis in the light of the Bader charge analysis, the latter reinforces the conjecture from the former that Cr shows a high preference for the Cr_2O_3 structure in which the Cr is in a +3 oxidation state.

Fe, on the other hand, appears to be only slightly more likely to be found in the +3 oxidation state than in lower oxidation states. In contrast to Cr, the number of nearest neighbors of Fe also shows a range, indicating that iron shows a range of preferred structures while Cr does not. This flexibility in structure and oxidation state on the part of Fe allows it to readily bond with available oxygen at the surface and allow that oxygen to diffuse through the oxide layer while undergoing changes in the number of nearest neighbors and oxidation state. By the same token, the ability of chromium to passivate steel appears to arise from its lack of flexibility in the number of nearest neighbors (i.e., preferred structure) and oxidation states.

IV. SUMMARY AND CONCLUSIONS

First principles DFT calculations are applied to gain insights into the structure and properties of the oxide layers formed when a FeCr alloy slab is oxidized. A Monte Carlo atom-swapping algorithm was employed to efficiently explore the large configuration space to identify the most favorable distribution of atoms. Although four different initial structures were used, the Monte Carlo approach yielded final structures that are quite close in energy and atomic distributions, confirming that the swapping algorithm is robust. The final energies of the structures were quite stable during the last several swapping steps, suggesting that the structures identified are likely to be the most favorable ones.

Analysis of the resulting structures show that the vacuum/oxide interface is rich in iron which is in a lower oxidation state, possibly reacting with oxygen to form FeO. Deeper into the oxide layers, the oxidation state of Fe becomes more positive, possibly forming Fe_2O_3 and perhaps also the mixed oxide Fe_3O_4. The analysis also shows that the preferred number of nearest neighbors of Fe covers a range between 0 and 6, implying that the iron oxide phases also exhibit flexibility in structure. The Cr, while not present at the surface, also bonds with oxygen. However, in contrast to Fe, the chromium atom prefers to be surrounded by 6 oxygen neighbors while remaining in a fixed oxidation state that is consistently more positive than that of Fe.

Based on these observations, we conclude that the passivation of steel by chromium results from a combination of the rigidity in its preferred oxidized structure and oxidation state.

V. ACKNOWLEDGEMENTS

REFERENCES

[1] M. Ropo *et al.*, "Theoretical evidence of the compositional threshold behavior of FeCr surfaces," *Phys. Rev. B - Condens. Matter Mater. Phys.*, vol. 76, no. 22, pp. 6–9, 2007.

[2] N. K. Das, K. Suzuki, Y. Takeda, K. Ogawa, and T. Shoji, "Quantum chemical molecular dynamics study of stress corrosion cracking behavior for fcc Fe and Fe-Cr surfaces," *Corros. Sci.*, vol. 50, no. 6, pp. 1701–1706, 2008.

[3] N. K. Das, K. Suzuki, K. Ogawa, and T. Shoji, "Early stage SCC initiation analysis of fcc Fe-Cr-Ni ternary alloy at 288 °C: A quantum chemical molecular dynamics approach," *Corros. Sci.*, vol. 51, no. 4, pp. 908–913, 2009.

[4] N. K. Das, T. Shoji, and Y. Takeda, "A fundamental study of Fe–Cr binary alloy–oxide film interfaces at 288°C by computational chemistry calculations," *Corros. Sci.*, vol. 52, no. 7, pp. 2349–2352, Jul. 2010.

[5] N. K. Das and T. Shoji, "Early stage oxidation initiation at different grain boundaries of fcc Fe-Cr binary alloy: A computational chemistry study," *Oxid. Met.*, vol. 79, no. 3–4, pp. 429–441, 2013.

[6] M. P. J. Punkkinen *et al.*, "Adhesion of the iron–chromium oxide interface from first-principles theory," *J. Phys. Condens. Matter*, vol. 25, no. 49, p. 495501, 2013.

[7] A. Kuronen *et al.*, "Segregation, precipitation, and α-α′ Phase separation in Fe-Cr alloys," *Phys. Rev. B - Condens. Matter Mater. Phys.*, vol. 92, no. 21, pp. 1–16, 2015.

[8] A. D. Becke, "Density-functional thermochemistry. II. The effect of the Perdew–Wang generalized-gradient correlation correction," *J. Chem. Phys.*, vol. 97, no. 12, pp. 9173–9177, Dec. 1992.

[9] C. Leygraf and G. Hultquist, "Initial oxidation stages on Fe-Cr(100) and Fe-Cr(110) surfaces," *Surf. Sci.*, vol. 61, no. 1, pp. 69–84, Dec. 1976.

[10] J. R. Lince, S. V. Didziulis, D. K. Shuh, T. D. Durbin, and J. A. Yarmoff, "Interaction of O2 with the Fe0.84Cr0.16(001) surface studied by photoelectron spectroscopy," *Surf. Sci.*, vol. 277, no. 1–2, pp. 43–63, 1992.

[11] H. J. Mathieu and D. Landolt, "An investigation of thin oxide films thermally grown on Fe-24Cr and Fe-24Cr-11Mo by Auger electron spectroscopy and X-ray photoelectron spectroscopy," *Corros. Sci.*, vol. 26, pp. 547–559, 1986.

[12] S. Suzuki, T. Kosaka, H. Inoue, M. Isshiki, and Y. Waseda, "Effect of the surface segregation of chromium on oxidation of high-purity Fe-Cr alloys at room temperature," *Appl. Surf. Sci.*, vol. 103, pp. 495–502, 1996.

[13] A. P. Greeff, C. W. Louw, and H. C. Swart, "The oxidation of industrial FeCrMo steel," *Corros. Sci.*, vol. 42, pp. 1725–1740, 2000.

[14] P. Stefanov, D. Stoychev, M. Stoycheva, and T. Marinova, "XPS and SEM studies of chromium oxide films chemically formed on stainless steel 316 L," *Mater. Chem. Phys.*, vol. 65, pp. 212–215, 2000.

[15] D. Mandrino, C. Donik, and M. Jenko, "AES of thin oxide layers on a duplex stainless steel surface," *Surf. Interface Anal.*, vol. 42, pp. 762–765, 2010.

[16] C. Donik, A. Kocijan, J. T. Grant, M. Jenko, A. Drenik, and B. Pihlar, "XPS study of duplex stainless steel oxidized by oxygen atoms," *Corros. Sci.*, vol. 51, pp. 827–832, 2009.

[17] C. Donik, A. Kocijan, D. Mandrino, I. Paulin, M. Jenko, and B. Pihlar, "Initial oxidation of duplex stainless steel," *Appl. Surf. Sci.*, vol. 255, pp. 7056–7061, 2009.

[18] C. Donik, D. Mandrino, and M. Jenko, "Depth profiling and angular dependent XPS analysis of ultra thin oxide film on duplex stainless steel," *Vacuum*, vol. 84, pp. 1266–1269, 2010.

[19] D. Mandrino and C. Donik, "Chemical-state information obtained by AES and XPS from thin oxide layers on duplex stainless steel surfaces," *Vacuum*, vol. 86, pp. 18–22, 2011.

[20] W. Fredriksson, S. Malmgren, T. Gustafsson, M. Gorgoi, and K.

Edström, "Full depth profile of passive films on 316L stainless steel based on high resolution HAXPES in combination with ARXPS," *Appl. Surf. Sci.*, vol. 258, pp. 5790–5797, 2012.

[21] J. R. Trelewicz, G. P. Halada, O. K. Donaldson, and G. Manogharan, "Microstructure and Corrosion Resistance of Laser Additively Manufactured 316L Stainless Steel," *Miner. Met. Mater. Soc.*, vol. 68, no. 3, pp. 850–859, 2016.

[22] J. Hafner, "Ab-initio simulations of materials using VASP: Density-functional theory and beyond," *J. Comput. Chem.*, vol. 29, no. 13, pp. 2044–2078, Oct. 2008.

[23] J. P. P. Perdew, K. Burke, and M. Ernzerhof, "Generalized Gradient Approximation Made Simple.," *Phys. Rev. Lett.*, vol. 77, no. 18, pp. 3865–3868, Oct. 1996.

[24] P. E. Blöchl, "Projector augmented-wave method," *Phys. Rev. B*, vol. 50, no. 24, pp. 17953–17979, 1994.

[25] G. Kresse and D. Joubert, "From ultrasoft pseudopotentials to the projector augmented-wave method," *Phys. Rev. B*, vol. 59, no. 3, pp. 1758–1775, Jan. 1999.

[26] J. G. Lee, *Computational Materials Science: An Introduction*. CRC Press, 2011.

[27] H. J. Monkhorst and J. D. Pack, "Special points for Brillouin-zone integrations," *Phys. Rev. B*, vol. 13, no. 12, pp. 5188–5192, 1976.

[28] R. F. W. Bader, "Atoms in molecules," *Acc. Chem. Res.*, vol. 18, pp. 9–15, 1985.

[29] G. Henkelman, "Bader code." [Online]. Available: http://theory.cm.utexas.edu/henkelman/code/bader/. [Accessed: 07-Jan-2017].

[30] G. Henkelman, A. Arnaldsson, and H. Jónsson, "A fast and robust algorithm for Bader decomposition of charge density," *Comput. Mater. Sci.*, vol. 36, no. 3, pp. 354–360, 2006.

[31] E. Sanville, S. D. S. D. Kenny, R. Smith, and G. Henkelman, "Improved grid-based algorithm for Bader charge allocation," *J. Comput. Chem.*, vol. 28, no. 5, pp. 899–908, Apr. 2007.

[32] W. Tang, E. Sanville, and G. Henkelman, "A grid-based Bader analysis algorithm without lattice bias.," *J. Phys. Condens. Matter*, vol. 21, no. 8, p. 084204, 2009.

[33] M. Yu and D. R. Trinkle, "Accurate and efficient algorithm for Bader charge integration," *J. Chem. Phys.*, vol. 134, no. 6, p. 064111, Feb. 2011.